

Synthesis, Structures and Properties of Benzoporphycenes and Naphthoporphycenes

Daiki Kuzuhara^a, Hiroko Yamada^{a,b,*}, Shigeki Mori^c, Tetsuo Okujima^d, and Hidemitsu Uno^d

Dedicated to Professor Karl Kadish on the occasion of his 65th birthday.

^a*Graduate School of Material Science, Nara Institute of Science and Technology, 8916-5 Takayama-cho, Ikoma 630-0192, Japan*

^b*CREST, JST, Chiyoda-ku 102-0075, Japan,*

^c*Department of Molecular Science, Integrated Center for Science, Ehime University, Matsuyama 790-8577, Japan*

^d*Graduate School of Science and Engineering, Ehime University, 2-5, Bunkyo-cho, Matsuyama, 790-8577, Japan*

Received date (to be automatically inserted after your manuscript is submitted)

Accepted date (to be automatically inserted after your manuscript is accepted)

ABSTRACT: A series of benzoporphycenes and naphthoporphycenes and their zinc complexes were prepared from bicyclo[2.2.2]octadiene fused porphycenes by a retro-Diels-Alder reaction and their photophysical properties were studied. Free-base tetranaphthoporphycene was not soluble in common organic solvents, but zinc tetranaphthoporphycene was slightly soluble in pyridine and showed B and Q bands at 507 and 690 nm, respectively. Dinaphthoporphycene showed broad B and Q bands due to its lower symmetry. Tetrabenzo-, dibenzo-, and dinaphthoporphycenes showed fluorescence at 673, 654, and 670 nm with quantum yields of 0.32, 0.42, and 0.31, respectively, although their precursors were non-fluorescent. Zinc complexes of tetrabenzo-, dibenzo-, tetranaphtho-, dinaphthoporphycenes and their bicyclo[2.2.2]octadiene-fused precursors revealed moderate fluorescence with quantum yields of 0.15-0.37. The crystal structures of tetrabenzo- and dibenzoporphycenes showed herringbone structures, while the zinc tetrabenzoporphycene showed a hexagonal box-structure with six pyridine ligands inside.

KEYWORDS: Porphycenes, retro Diels-Alder reaction, crystal structure, fluorescence spectra

*Graduate School of Material Science, Nara Institute of Science and Technology, 8916-5, Takayama-cho, Ikoma, Nara 630-0192, JAPAN. Tel: +81-743-72-6041; Fax: +81-743-72-6042; E-mail: hyamada@ms.naist.jp

INTRODUCTION

Isomeric porphyrins, which have a 18π aromatic macrocycle-structure consisting of four pyrroles and four *meso*-like bridge carbons with $C_{20}H_{14}N_4$ skeleton, have been reported in the past 30 years; namely [18]porphyrin(2.0.2.0) (porphycene) [1], [18]porphyrin(2.1.0.1) (corrphycene) [2], [18]porphyrin(2.1.1.0) (hemiporphycene) [3] and [18]porphyrin(3.0.1.0) (isoporphycene) [4]. The variety of the structures of these isomers influenced not only the metal coordination properties due to the inner N₄ cavity size, but also the optical properties due to the difference of molecular symmetries. Vogel and coworkers reported the first characterized example of the porphyrin isomers, porphycene, in 1986¹. The porphycene was observed to contain the structure features reminiscent of porphyrins and acenes. This led Vogel to propose the name “porphycene” for these compounds [5, 6].

Porphycenes have shown unique optical properties due to their lower symmetry compared to those of porphyrins. Porphycenes generally display intense absorption bands in the NIR regions. These optical properties have been investigated for their applications in the fields of photodynamic therapy (PDT), catalysis, protein mimicry, and material chemistry [7].

Most of the porphycene derivatives have been prepared from 5,5'-diformyl-2,2'-bispyrrole derivatives by a McMurry coupling reaction. In particular, 2,7,12,17-tetrapropyl substituted porphycene (TPrPc) [8] has been the most studied structure and has played a dominant role in the porphycene chemistry as an octaethylporphyrin in the porphyrin chemistry, because TPrPc is soluble in common organic solvents and can give nice crystals. β,β' -Octaalkyl-substituted porphycenes [9] have been reported by Vogel and coworkers. They revealed a slightly twisted macrocyclic framework. The shape of four pyrrolic nitrogen atoms in the core of octaethylporphycene (OEPc) showed a nearly square and planar arrangement. By contrast, the four pyrrolic nitrogen atoms of TPrPc were found to be a rectangular orientation. The positions of peripheral porphycene substituents influenced the size and the shape of the inner N₄ cavities [10].

Although, many kinds of alkyl- or aryl-substituted porphycenes have been reported [11], π -expanded porphycenes have rarely been reported. Vogel and coworkers reported the first example of π -expanded porphycenes; the dibenzoporphycenes annulated with benzene rings at 3,6- and 13,16-positions [12]. Recently, Sessler's group and Panda's group independently [13] reported dinaphthoporphycenes where the benzene rings were replaced by naphthalenes. In addition, the porphycene frameworks annulated with a benzene ring at 2,20- or 9,10-positions have been also reported [14, 15]. Interestingly, the absorption spectra of these π -expanded porphycenes showed bathochromic shifts compared to those of the parent porphycenes. In contrast, only one example of

[2.3]benzoporphycene, where an aromatic ring was annulated with pyrrolic β -positions on porphycene core, has been reported to date [16].

Recently, we have developed a synthesis of tetrabenzoporphyrins (TBPs) [17,18] and a variety of other ring-fused expanded porphyrinoids such as naphtho-, anthra- and benzofluorantho-porphyrins [19-21], core-modified porphyrins [22] and sapphyrins [23], based on retro-Diels–Alder reactions of peripheral bicyclo[2.2.2]octadiene (BCOD) substituents. These BCOD precursors were dissolved in common organic solvents, and could be purified by column chromatography and crystallization. When the retro-Diels–Alder reaction is performed, the conversion does not need chemical reagents, and only heating is necessary. In addition, this method can be applied to solution processable devices [24]. Retro-Diels–Alder reaction of the precursors of TBPs at 200 °C after spin coating gave the corresponding semiconducting films, which showed good mobilities as high as $\mu_{\text{FET}} = 0.2 \text{ cm}^2 \text{ V}^{-1} \cdot \text{s}^{-1}$ for NiTBP [25]. This is a very good performance for solution processable and small molecule semiconductors. Soluble precursors were used not only for OFETs but also for thin film organic photovoltaics (OPVs). Solution-processable fabrication afforded p-i-n OPV devices composed of BP and bis(dimethylphenylsilylmethyl)[60]fullerenes (SIMEF), with a respectable performance of 5.2% photoenergy conversion efficiency [26].

In 2009, we have reported a preparation of tetrabenzoporphycene (**2-H₂**) and dibenzoporphycene (**4-H₂**) by retro-Diels–Alder reaction of BCOD-fused porphycenes, **1-H₂** and **3-H₂**, respectively (Figure 1) [27]. No fluorescence emission was observed for **1-H₂** and **3-H₂** in CH₂Cl₂, but **2-H₂** and **4-H₂** emitted strongly at 673 and 654 nm with 0.32 and 0.42 quantum yields, respectively. Using this retro-Diels–Alder reaction method, we have also succeeded to prepare dodeca-substituted porphycene and 9,10,19,20-tetraalkylsubstituted-tetrabenzoporphycenes for the first time [28]. Here we will apply this method to prepare further π -expanded porphycenes, tetranaphthoporphycene (**6-H₂**), dinaphthoporphycene (**8-H₂**), and their zinc complexes (**6-Zn** and **8-Zn**), to see their photophysical properties comparing with those of **1-H₂** and **3-H₂**, and their zinc complexes (Figure 1). The crystal structures of **2-H₂**, **2-Zn** and **4-H₂** will be also discussed.

Figure 1

RESULTS AND DISCUSSION

Synthesis of benzoporphycenes and naphthoporphycenes

The synthesis of free-base tetrabenzo- and dibenzoporphycenes (**2-H₂** and **4-H₂**) has been already reported in the literature [27]. The synthesis of tetranaphthoporphycenes **6-H₂** and dinaphthoporphycenes **8-H₂** are summarized in Scheme 1 and 2. Pyrrole **9** [19] was treated with

benzyltrimethylammonium iodine dichloride (BTMA•ICl₂) to give iodopyrrole **10** in 95% yield. After pyrrolic NH of **10** was protected with *tert*-butoxycarbonyl (Boc) group, the pyrrole **11** was dimerized by an Ullmann coupling reaction. The Boc group of the crude product **12** was deprotected with conc. HCl to give bispyrrole **13** in 68% in 2 steps. After decarboxylation, the α positions of **14** were formylated by a Vilmeyer reaction to give diformyl-bispyrrole **15** in 93% yield.

Scheme 1

The dimerization of bispyrrole **15** by a McMurry coupling reaction afforded porphycene **5-H₂** in 10% yield. The hetero coupling of bispyrrole **15** and bispyrrole **16** [27] gave **7-H₂** in 7% yield after purification by column chromatography (Scheme 2) with porphycene **5-H₂** in 3% and 2,7,12,17-tetrahexylporphycene **17** in 7%. From thermogravimetric analysis of **5-H₂** (Figure 2), the retro-Diels-Alder reaction started at around 216 °C and ended at 306 °C. The weight loss of **5-H₂** was 14% and was comparable with the calculated values of 14%. Porphycenes **5-H₂** and **7-H₂** were quantitatively converted into tetranaphthoporphycenes **6-H₂** and **8-H₂** at 300 °C in vacuo. However porphycene **5-H₂** was not soluble in any common organic solvents such as CHCl₃, CH₂Cl₂, TFA, hot toluene, therefore its ¹H NMR and UV-vis absorption spectra were not available.

Scheme 2

Figure 2

Zinc porphycene **1-Zn** and **5-Zn** were prepared from **1-H₂** and **5-H₂** by treatment with Zn(OAc)₂•2H₂O in CHCl₃ at 50 °C in the presence of TEA. The expanded porphycene **2-Zn** and **6-Zn** were prepared from porphycenes **1-Zn** and **5-Zn** quantitatively by heating at 220 °C and 290 °C, respectively. The conversion of **3-H₂** and **7-H₂** to the corresponding zinc complexes was unsuccessful, and only the starting materials were recovered. The similar results have been reported by Vogel [8, 9]. 2,7,12,17-Tetrapropylporphycene could not be converted to the corresponding zinc complex because the shape of the inner N₄ core was rectangular and the inner nitrogen cavity was small. Expanded porphycenes **3-H₂** and **8-H₂**, however, were successfully converted to the zinc complexes of **3-Zn** and **8-Zn** with Zn(OAc)₂•2H₂O in refluxed DMF in 83 and 81% yield, respectively.

Scheme 3

Photophysical properties of benzoporphycenes and naphthoporphycenes

The UV-vis-NIR absorption spectrum of **8-H₂** in CH₂Cl₂ is shown in Figure 3 with those of the reference porphycenes **4-H₂**, **7-H₂** and **17**. The photophysical data is also summarized in Table 1. The UV-vis-NIR absorption spectrum of **7-H₂** was similar to that of **3-H₂** with the B peak at 373 nm with shoulder at 384 nm, therefore only the spectrum of **7-H₂** is shown in Figure 3. The reference **17** had a B peak at 371 nm but the shoulder at 383 nm was relatively small. The Q band peaks of **7-H₂** were observed at 567, 610, and 642 nm and were slightly red-shifted from 563, 601, and 633 nm of reference **17** and 561, 606, and 640 nm of **3-H₂**. After the retro-Diels-Alder reaction, the B and Q peaks of the π -expanded dinaphthoporphycene **8-H₂** were further red-shifted compared to the corresponding precursor **7-H₂**. The B peaks of **8-H₂** showed vibration bands clearly and the peaks were observed at 395, 413, 435, and 462 nm. The strongest B peak was red-shifted by 91 nm from those of **7-H₂** and **17**, and by 52 nm from that of dibenzoporphycene **4-H₂**. The Q band peaks of **8-H₂** were observed at 602, 637, and 659 nm. The strongest Q band peak of **8-H₂** was red-shifted from those of **7-H₂** and **17** by 12 and 25 nm, respectively. The relative intensity of Q band to B band was stronger than those of BCOD porphycenes and porphycene **17** due to its π -expansion. For the benzoporphycene **4-H₂**, the addition of benzo groups to porphycene core lead the red-shift of B and Q bands compared to **17**, because of the π -expansion [27]. Further addition of benzo groups to the peripheral phenyl rings, to form **8-H₂**, induced the further red-shift of the Q and B bands. The Q₀₀ band was stronger with the increased fused phenyl rings, due to the electric dipole allowance by the lowered structure symmetry [27].

The DFT calculations of **2-H₂**, **6-H₂**, **4-H₂**, **8-H₂**, and the parent porphycene without peripheral substituents (**PcH₂**) were performed with Gaussian 03 at the B3LYP/6-31G* levels [29]. The MO energies with $|\Delta\text{LUMO}-\Delta\text{HOMO}|$ values are shown in Figure S1 and their four frontier molecular orbital are shown in Figure S2. The asymmetry of MO orbitals increased from **PcH₂** to **4-H₂** and **8-H₂**, which agreed with the results of UV-vis absorption spectra.

Figure 3

Table 1

The fluorescence of BCOD precursors, **3-H₂** and **7-H₂**, was not observed at rt. These phenomena have been generally observed for the free-base β,β' -alkyl-substituted porphycenes [30]. The reason has been predicted by Waulk et al that the radiationless channel is provided by crossing of the potential energy surfaces of the ground and lowest excited states along the hydrogen-transfer

coordinates [30b]. After a retro-Diels-Alder reaction of **7-H₂**, the fluorescence of **8-H₂** was strongly observed at 670 nm with a shoulder at 720 nm with quantum yield of 0.31, as shown in Figure 2. The foot of the fluorescence reached to 900 nm. Similarly, the fluorescence of **4-H₂** showed two peaks at 654 and 726 nm with quantum yield of 0.42. This drastic change of the fluorescence before and after retro-Diels-Alder reaction was also observed for **1-H₂** and **2-H₂** [27].

Figure 4

The absorption spectra of zinc complexes **2-Zn** and **6-Zn** in pyridine are shown in Figure 5 with those of BCOD precursors **1-Zn** and **5-Zn**. The absorption spectra of **1-Zn** and **5-Zn** showed similar shapes. The B and Q bands were observed at 391, 595 and 638 nm for **1-Zn** and 392, 598 and 642 nm for **5-Zn** (Figure 5). When the BCOD-fused porphycenes were replaced to benzo- or naphthoporphycenes, the B and Q bands exhibited red-shifts. The B band of **2-Zn** and **6-Zn** are red-shifted by 54 and 116 nm, whereas the Q bands are red-shifted by almost 14 and 44 nm from those of BCOD precursors **1-Zn** and **5-Zn**, respectively. The DFT calculations of **2-Zn**, **6-Zn**, **4-Zn**, **8-Zn**, and the parent porphycene without peripheral substituents (**PcZn**) performed with Gaussian 03 at the B3LYP/6-31G* levels are shown in Figure S3. Their MO energies with $|\Delta\text{LUMO}-\Delta\text{HOMO}|$ values are shown in Figure S1. The Q₀₀ bands are significantly weaker in the case of **2-Zn** and **6-Zn**, because the $|\Delta\text{LUMO}-\Delta\text{HOMO}|$ values predicted for the porphycene π -system were lowered upon substitution with the fused benzene rings, as theoretically predicted before [27]. The vibration structure of Q bands of zinc porphycenes is more simple than that of free-base porphycene, due to the higher structure symmetry, as is also observed for porphyrins.

Figure 5

The UV-vis spectra of dibenzo- and dinaphthoporphycenes **4-Zn** and **8-Zn** are shown in Figure 6 with that of **1-Zn**. The B and Q bands of **4-Zn** were observed at 424 and 643 nm, which were red-shifted by 33 and 6 nm from those of **1-Zn**, respectively. The dinaphthoporphycene **8-Zn** showed split B bands between 440 and 490 nm and the intense Q band at 659 nm. The red-shift of **8-Zn** depends on the increased number of annulated benzene rings attached porphycene core. At the same time the lower symmetry by the fused phenyl rings introduced the splitting of the B band of **8-Zn**.

Figure 6

The normalized emission spectra of zinc complexes in pyridine are shown in Figure 7. The BCOD precursor **1-Zn** showed emission spectra with two bands at 648 and 701 nm with quantum yield of 0.26 by excitation at the B band. Similarly **5-Zn** showed emission spectra at 656 and 709 nm with quantum yield of 0.28. Although **1-H₂** and **5-H₂** showed very weak fluorescence, zinc porphycenes **1-Zn** and **5-Zn** showed strong fluorescence in NIR regions. On the other hand, zinc benzoporphycenes showed the emission peaks at 654 and 710 nm for **2-Zn** and 659 and 724 nm for **4-Zn**, and the emission quantum yields were 0.37 and 0.32, respectively. In the cases of naphthoporphycene **6-Zn** and **8-Zn**, the emission peaks showed more red-shifted than those of benzoporphycene **2-Zn** and **4-Zn**. The naphthoporphycenes exhibited the emission at 696 and 764 nm for **6-Zn** and 671 and 735 nm for **8-Zn** and the quantum yields were 0.17 and 0.15, respectively.

Figure 7

Crystal Structure of benzoporphycenes

Crystal structure of **2-H₂** is shown in Figure 8. Single crystals of **2-H₂** suitable for X-ray diffraction analysis was obtained by slow evaporation of the mother liquor from the CS₂ solution of **2-H₂**. There were two crystallographically independent molecules of **2-H₂** in a unit cell. Each **2-H₂** molecule was flat and N1-N2 and N2-N3 distances are 2.767(4) and 2.819(4) for molecule 1 and 2.772(4) and 2.801(4) Å for molecule 2. The C3-C6 distance was 3.385(4) Å and 3.322(4) Å and C19-C20 distance was 1.388(4) Å and 1.386(4) Å for molecules 1 and 2, respectively. The inner angles at C 19 and C20 were 132.0(3)° and 132.5(3)° for molecule 1 and 132.0(3)° and 131.9(3)° for molecule 2. The shape of rectangular N4 cavity depends on the peripheral substituents. The porphycene **2-H₂** shows longer N2-N3 side, which is similar to β,β' -octaethylporphycene (N1-N2 = 2.732 Å and N2-N3 = 2.799 Å) [31] and opposite to **1-H₂** (N1-N2 = 2.805 Å and N2-N3 = 2.694 Å).²⁸ Because of the steric hindrance between phenyl rings, C3 and C8 were kept away and therefore the N1-N2 distance was shorter compared to **1-H₂**. The packing structure of the molecules in single crystals was herringbone type. This is the similar structure with pentacene, which is well-known p-type organic semiconductor molecule. The π -planes of two parallel **2-H₂** molecules were piled up and the distances between parallel **2-H₂** molecules were 3.330 and 3.294 Å for molecules 1 and 2, respectively. These values suggested π - π interactions between parallel molecules. The dihedral angle of neighboring porphycene molecules was 74.06°. A minimum distance between outer hydrogen atoms of benzene rings and the neighboring porphycene π -plane was 2.746(3) Å and there was an H- π electronic interaction.

Figure 8

Crystal structure of **4-H₂** is shown in Figure 9. Single crystals of **4-H₂** suitable for X-ray diffraction analysis were obtained by slow diffusion of MeOH into a solution of **4-H₂** in CH₂Cl₂. Two benzopyrrole rings were bent by 8.43° due to the steric hindrance between facing hydrogen atoms of phenyl rings. The N1-N2 distance was 2.798(3) Å and N3-N4 distance was 2.862(3) Å, therefore the shape of the N4 cavity was a trapezoid. Because of the steric hindrance between phenyl pyrroles, N1-N2 distance is shorter than N3-N4 distance. The N2-N3 and N4-N1 distances were 2.666(3) and 2.679(3) Å, which are similar to non-substituted porphycene and β-tetraalkylporphycenes, due to the smaller steric hindrance between hexyl-pyrroles. The distance between parallel N4 planes was 3.258 Å and the mutual angle between N4 plane was 89.96°. The packing structure of **4-H₂** was herringbone, with hexyl tails alternately stuck out in opposite direction. A minimum distance between outer hydrogen atoms of benzene rings and the neighboring porphycene π-plane was 2.730(2) Å and there was an H-π electronic interaction.

Figure 9

Vogel and co-workers have found that the peripheral alkyl substituents of porphycene effect the geometry of the ring skeleton and the shape and size of the N₄-coordination hole [10]. The strength of N-H...N hydrogen bonding between ethynyl-linked pyrrolic nitrogen atoms can be observed by chemical shift of NH protons and the N-N distances can be estimated by X-ray crystal structure analysis. Generally the chemical shifts of porphyrin NH protons were observed in relatively higher magnetic field because of the ring current of porphyrin aromatic macrocycles. However, the N-H...N hydrogen bonding between the nitrogen atoms of porphycenes is stronger compared to those of porphyrins and the chemical shift of the inner NH proton shows the lower magnetic field shift. There was a good correlation between NH-chemical shift and N-N distances. The N-N cavity of β,β'-octaalkyl porphycene was close to square and the the N-H...N hydrogen bonding was weak with chemical shift at around 1.0 ppm.²⁸ The *meso*-substituted porphycenes were rectangular and the N-H...N hydrogen bonding was strong with chemical shift at around 5.5-7.0 ppm. For **4-H₂** the NH chemical shift was 2.7 ppm, which is similar to 3.0 ppm of β-tetraethyl porphycene and non-substituted porphycene [28]. Although the substituents were two fused phenyl rings and two hexyl groups with trapezoidal N-4 cavity, the relationship between NH chemical shifts and N-N distances were well agreed with other alkyl-substituted porphycenes [28]. The fluorescence attitude of **4-H₂**

with fluorescence quantum yield of 0.42 was also similar to β -tetraethyl porphycene and non-substituted porphycene, while *meso*-substituted and β,β' -octaalkyl porphycenes were non-fluorescent.

Crystal structure of **2-Zn** is shown in Figure 10. Single crystal of **2-Zn** suitable for X-ray diffraction analysis was obtained by slow diffusion of MeOH into a solution of **2-Zn** in pyridine. One pyridine molecule was coordinated to the zinc ion and the porphycene showed a shallow dome-shape. Zinc ion was risen by 0.357 Å from N4 plane and Zn-N(pyridine) distance was 2.127(1) Å, which is shorter than that of zinc complex of β,β' -octaethyl porphycene, 2.158 Å [31]. The N1-N2 and N2-N3 distances were 2.638(3) and 3.062(3) Å, showing rectangular shape compared to the almost square shape of free base porphycene **2-H₂**. The Zn-N distances were 2.046-2.059 Å, which was longer than that of zinc complex of β,β' -octaethyl porphycene and similar to zinc porphyrinate [31]. The porphycene plane gave saddle-shape structure and the angles between neighboring pyrroles were 2.10° for ethylene-bridged pyrroles and 12.36° for directly connected pyrroles. Six **4-Zn** molecules were assembled to make a hexahedral box-structure with six coordinated pyridine molecules inside. The angles between N4 planes of neighboring **4-Zn** molecules were all 83.10° and the distance between parallel planes was 11.872 Å. The angles between neighboring pyridine π -planes were all 71.36°. The distances of the neighboring boxes at faced N4 planes were 3.510 Å. Such a cage-type structure of porphyrins has been reported for a zinc opp-dibenzoporphyrin with an axial pyridine-ligand. The eight porphyrin molecules gave octahedral structure with eight pyridine ligands inside of the cage [32].

Figure 10

EXPERIMENTAL

General

Melting points were measured with Yanaco MP500-D apparatus and were not corrected. Decomposition temperatures were measured on an SII Exstar 600 TG/DTA 6200. ¹H and ¹³C NMR spectra were recorded on a JEOL JNM-AL 400 and JNM-EC P 400 spectrometer at ambient temperature using tetramethylsilane as an internal standard. FAB and DI-EI mass spectra were measured on a JEOL JMS-700 spectrometer, and a Voyager DE Pro (Applied Biosystems) spectrometer was used for MALDI-TOF measurements using dithranol as the matrix. ESI-MS spectra were measured with a mass spectrometer JEOL JMS-T100LC AccuTOF. Elemental analyses were performed with a Yanaco MT-5 elemental analyzer. Thin-layer chromatography

(TLC) and column chromatography were performed on Art. 5554 (Merck KGaA) and Silica Gel 60N (Kanto Chemical Co.), respectively. All solvents and chemicals were reagent grade quality, obtained commercially and used without further purification except as noted. For spectral measurements, spectral grade of CH₂Cl₂ and pyridine were purchased. Steady state absorption spectra in the visible and near-IR regions were measured on a JASCO V570. Steady-state fluorescence spectra were measured on Absolute PL Quantum Yield Measurement System C9920-02.

Synthesis

Synthesis of porphycenes **1-H₂**, **2-H₂**, **3-H₂**, **4-H₂**, and **17** have been already reported.²⁷

Ethyl 4,11-hydro-4,11-ethano-3-iodo-2*H*-benzo[*f*]isoindole-1-carboxylate (**10**)

A mixture of isoindole **9** [19] (2.95 g, 11 mmol), BTMA•ICl₂ (4.18 g, 12 mmol) and CaCO₃ (2.2 g, 22 mmol) in CH₂Cl₂ (100 ml) and MeOH (50 ml) was refluxed for 2 h. After cooling to rt, the precipitate was filtered off and washed with CH₂Cl₂. The combined filtrate was washed with saturated aqueous NaHSO₃, water and brine, and then was dried over Na₂SO₄. After a removal of the solvent, the crude product was crystallized from CHCl₃/hexane to give **10** as a white powder. Yield 95% (4.11 g, 10.4 mmol). mp 214.4 °C. ¹H NMR (400 MHz; CD₂Cl₂): δ_H, ppm 8.77 (brs, 1H, NH), 7.25-7.21 (m, 2H, benzo), 7.10-7.07 (m, 2H, benzo), 4.75 (s, 1H, bridge head), 4.32 (q, 2H, *J* = 7.1 Hz, CO₂CH₂CH₃), 4.06 (s, 1H, bridge head), 1.69 (m, 4H, bridge), 1.38 (t, 3H, *J* = 7.1 Hz, CO₂CH₂CH₃). ¹³C NMR (100 MHz; CD₂Cl₂): δ_C, ppm 160.61, 144.55, 144.13, 137.05, 136.62, 125.88, 123.86, 123.54, 119.93, 62.77, 60.67, 38.55, 38.36, 27.85, 27.40, 14.71. MS (FAB): *m/z* 394 [M⁺]. Anal. calcd for C₁₇H₁₆INO₂: C, 51.93; H, 4.10; N, 3.56%. Found: C, 51.69; H, 4.06; N, 3.58.

Ethyl 4,11-hydro-4,11-ethano-3-iodo-2*N*-Boc-benzo[*f*]isoindole-1-carboxylate (**11**)

To a solution of **10** (3.83 g, 9.7 mmol), *p*-dimethylaminopyridine (DMAP) (70 mg), in CH₂Cl₂ (50 ml) was added (Boc)₂O (2.66 ml, 11.6 mmol), followed by stirring for 12 h at rt under an Ar atmosphere. The reaction mixture was washed with water and brine and then dried over Na₂SO₄. After a removal of the solvent, the crude product was purified by silica gel column chromatography (CH₂Cl₂). Crystallization from MeOH gave **11** as a white solid. Yield 87% (4.17 g, 8.46 mmol). mp 100.5 °C. ¹H NMR (400 MHz; CDCl₃, Me₄Si) δ_H, ppm 7.25-7.23 (m, 2H, benzo), 7.12-7.11 (m, 2H, benzo), 4.65 (s, 1H, bridge head), 4.31 (m, 2H, CO₂CH₂CH₃), 4.07 (s, 1H, bridge head), 1.71 (m, 4H, bridge), 1.58 (s, 9H, Boc), 1.39 (t, 3H, *J* = 7.1 Hz, CO₂CH₂CH₃). ¹³C NMR (100 MHz; CDCl₃, Me₄Si): δ_C, ppm 159.65, 148.98, 143.18, 142.76, 139.37, 137.96, 125.92, 125.89, 123.78, 123.44,

121.03, 85.30, 66.60, 60.53, 38.29, 38.15, 27.92, 27.62, 27.02, 26.64, 14.53. MS (FAB): m/z 494 $[M]^+$. Anal. calcd for $C_{22}H_{24}INO_4$: C, 53.45; H, 4.90; N, 2.84%. Found: C, 53.45; H, 4.83; N, 2.89.

1,1'-bis(4,9-ethano-10-ethoxycarbonyl 4,9-dihydro-benzo[f]isoindole) (13)

A mixture of **11** (3.95 g, 8.0 mmol) and Cu (4.0 g) in DMF (15 ml) was heated at 110 °C for 15 h under an Ar atmosphere. The reaction mixture was cooled to rt, then filtered through Celite to remove the copper, and washed with CH_2Cl_2 . The filtrate was washed with 1 M HCl, water and brine, dried over Na_2SO_4 , and the solvent was removed under a reduced pressure. The residue was purified by silica gel column chromatography (5% EtOAc/ CH_2Cl_2) to give crude *N*-Boc-bispyrrole **12**. The crude **12** was used without further purification in the next step. To a solution of crude bispyrrole **12** in EtOAc (60 ml) was added conc. HCl (20 ml) at rt. The mixture was stirred for 14 h at rt, then water was added. The mixture was extracted with EtOAc, and the extract was washed with saturated aqueous $NaHCO_3$, water and brine then dried over Na_2SO_4 . After a removal of the solvent, the crude product was purified by silica gel column chromatography (5% EtOAc/DCM) and crystallized from $CHCl_3$ /hexane to give **13** as a white powder. Yield 68% (1.48 g, 2.8 mmol). 1H NMR (400 MHz; $CDCl_3$; Me_4Si ; diastereomixture) δ_H , ppm 9.16 (br, 2H, *NH*), 7.44-7.08 (m, 8H, benzo), 4.83 (m, 2 H, bridge head), 4.45 (m, 2H, bridge head), 4.28 (m, 4H, $CO_2CH_2CH_3$), 1.90-1.71 (m, 8H, bridge), 1.36 (m, 4H, $CO_2CH_2CH_3$). ^{13}C NMR (100 MHz; $CDCl_3$, Me_4Si ; diastereomixture; typical signals) δ_C , ppm 161.93, 144.84, 144.78, 144.57, 144.49, 137.02, 129.24, 129.01, 125.94, 125.88, 125.83, 124.03, 123.94, 123.46, 123.35, 119.77, 119.72, 115.36, 60.70, 38.43, 37.94, 37.90, 28.31, 28.19, 27.65, 27.61, 14.66. HRMS (ESI): m/z 555.2261 (calcd. for $C_{34}H_{32}N_2O_4Na$ $[M+Na]^+$ 555.2260).

1,1'-bis(4,9-ethano-4,9-dihydro-benzo[f]isoindole) (14)

A mixture of **13** (1.3 g, 2.4 mmol) and NaOH (1.0 g) in ethylene glycol (30 ml) was heated at 170 °C for 1 h under an Ar atmosphere in the dark. After cooling to rt, the reaction mixture was poured into saturated aqueous $NaHCO_3$, and then extracted with EtOAc. The extract was washed with water and brine, dried over Na_2SO_4 , and the solvent was removed under a reduced pressure. The crude product was purified by silica gel column chromatography (CH_2Cl_2). Crystallization from $CHCl_3$ /hexane gave **14** as a pale blue solid. Yield 87% (0.82 g, 2.1 mmol). 1H NMR (400 MHz; CD_2Cl_2 ; diastereomixture): δ_H , ppm 7.53 (brs, 2H, *NH*), 7.34-7.05 (m, 8H, benzo), 6.56 (m, 2H, α -H), 4.32-4.27 (m, 4H, bridge head), 1.79-1.71 (m, 8H, bridge). ^{13}C NMR (100 MHz; $CDCl_3$, Me_4Si ; diastereomixture; typical signals): δ_C , ppm 145.86, 145.56, 129.80, 125.58, 125.34, 123.43, 123.38, 116.45, 108.80, 38.02, 37.69, 28.80, 28.73; HRMS (ESI): m/z 411.1837 (calcd. for $C_{28}H_{24}N_2Na$ $[M+Na]^+$ 411.1837).

1,1'-bis(4,9-ethano-4,9-dihydro-10-formyl-benzo[f]isoindole) (15)

To a solution of **14** (0.78 g, 2.0 mmol) in a mixture of DMF (5 ml) and CH₂Cl₂ (20 ml) was added POCl₃ (0.73 ml, 8.0 mmol) at 0 °C under an Ar atmosphere. The mixture was refluxed for 1 h. Aqueous sodium acetate (2.1 g / 30 ml of water) was carefully added to a reaction mixture at rt and refluxed for another 1 h. After cooling to rt, the mixture was extracted with CH₂Cl₂. The combined organic extracts was washed with saturated aqueous NaHCO₃, water and brine, and dried over Na₂SO₄. After a removal of the solvent under a reduced pressure, the crude product was purified by silica gel column chromatography (20% EtOAc in CH₂Cl₂). Crystallization from CH₂Cl₂/MeOH gave **15** as a pale yellow powder. Yield 93% (0.83 g, 1.9 mmol). ¹H NMR (400 MHz; DMSO-*d*₆, Me₄Si) δ_H, ppm 11.39 (brs, 1H, *NH*), 11.35 (brs, 1H, *NH*), 9.71 (s, 1H, *CHO*), 9.70 (s, 1H, *CHO*), 7.43-7.10 (m, 8H, benzo), 4.87 (brs, 2H, bridge head), 4.48 (m, 2H, bridge head), 1.87-1.70 (m, 8H, bridge). ¹³C NMR (100 MHz; DMSO-*d*₆; Me₄Si; typical signals): δ_C, ppm 177.06, 143.98, 143.52, 143.50, 129.50, 129.41, 129.22, 125.56, 125.53, 125.45, 125.15, 125.14, 123.53, 123.06, 122.78, 121.92, 121.83, 37.02, 36.98, 35.99, 27.51, 27.46, 27.05, 27.03; MS (FAB): *m/z* 445 [M⁺+1]; Anal. calcd for C₃₀H₂₄N₂O₂+1/3CH₂Cl₂: C, 77.05; H, 5.26; N, 5.92%. Found: C, 77.29; H, 5.83; N, 5.89.

Porphycene 5-H₂

TiCl₄ (0.83 ml, 7.6 mmol) was added dropwise to a THF (50 ml) solution containing Zn dust (0.98 g) and CuCl (48 mg, 0.48 mmol) at rt and the reaction mixture then was refluxed for 2 h. Subsequently a solution of **15** (0.13 g, 0.3 mmol) in THF (50 ml) was added dropwise to the boiling reaction mixture over 1 h. The mixture was then refluxed for another 30 min. After cooling to 0 °C, a 6% NH₃ aqueous solution (30 ml) was added dropwise. The precipitate was filtrated through a Celite pad, and washed with CH₂Cl₂. The filtrate was dried over Na₂SO₄, and the solvent was then removed under reduced pressure. The crude product was purified by silica gel chromatography (CH₂Cl₂). Recrystallization from CHCl₃/MeOH afforded **5-H₂** as a purple crystal. Yield 10% (12 mg, 15 μmol); mp 216 °C (decomposed). ¹H NMR (400 MHz; CDCl₃, Me⁴Si; diastereomixture): δ_H, ppm 9.91-9.87 (m, 4H, *meso*), 7.97-7.10 (m, 16H, aromatic), 6.52-6.48 (m, 4H, bridge head), 5.94-5.91 (4H, bridge head), 2.44-1.77 (m, 16H), 1.18 and 1.12 (brs, 2H, *NH*). UV-vis (CH₂Cl₂): λ_{max}, nm (logε) 373 (5.08), 386 (5.14), 573 (4.55), 618 (4.40), 652 (4.54). MS (MALDI-TOF): *m/z* 823 [M⁺], 795 [M⁺-C₂H₄], 795 [M⁺-C₂H₄], 766 [M⁺-2C₂H₄], 741 [M⁺-3C₂H₄], 710 [M⁺-4C₂H₄]. Anal. calcd for C₆₀H₄₆N₄+1/2H₂O: C, 86.61; H, 5.69; N, 6.73%. Found: C, 86.81; H, 5.69; N, 6.58.

Porphycene 6-H₂

Porphycene **5-H₂** was heated to 250 °C in the solid phase under a vacuum for 30 min. After cooling to rt, **6-H₂** was obtained quantitatively. Dark green solid. m.p. > 300 °C. ¹H NMR and ¹³C NMR spectra were not recorded because of poor solubility in common organic solvents.

Porphycene 7-H₂

TiCl₄ (2.74 ml, 25 mmol) was added dropwise to a THF (100 ml) solution containing Zn dust (3.27 g) and CuCl (0.20 g, 2.0 mmol) at rt and the reaction mixture was refluxed for 2 h. Subsequently a solution of **15** (0.22 g, 0.5 mmol) and **16** (0.18 g, 0.5 mmol) in THF (100 ml) was added dropwise to the boiling reaction mixture over 30 min. The mixture was then refluxed for another 30 min. After cooling to 0 °C, a 6% NH₃ aqueous solution (100 ml) was added dropwise. The precipitate was filtrated through a Celite pad, and washed with CH₂Cl₂. The filtrate was dried over Na₂SO₄, and the solvent was then removed under a reduced pressure. The crude product was purified by silica gel chromatography (25% CH₂Cl₂ in hexane). Recrystallization from CH₂Cl₂/MeOH afforded **6** as a purple crystal. Yield 7% (27 mg, 36 μmol). mp 227 °C (decomposed). ¹H NMR (400 MHz; CDCl₃, Me₄Si; diastereomixture): δ_H, ppm 9.88 (m, 2H, *meso*), 9.74 and 9.72 (d, 2H, *J* = 11 Hz, *meso*), 9.30 and 9.28 (s, 2H, β-position), 7.95-7.67 (m, 4H, aromatic), 7.37-7.19 (m, 4H, aromatic), 6.58-6.55 (m, 2H, bridge head), 5.93 (m, 2H, bridge head), 4.04 (m, 4H, CH₂C₅H₁₁), 2.46-2.25 (m, 10H, bridge+ CH₃CH₂C₄H₉), 2.10 (brs, 2H, -NH), 1.98 (m, 2H, bridge), 1.78 (m, 4H, -C₂H₄CH₂C₃H₇), 1.54 (m, 4H, -C₃H₆CH₂C₂H₅), 1.43 (m, 4H, -C₄H₈CH₂CH₃), 0.96 (m, 6H, -C₃H₁₀CH₃). UV-vis (CH₂Cl₂): λ_{max}, nm (logε) 373 (5.13), 384 (5.08), 567 (4.56), 609 (4.46), 642 (4.63); MS (MALDI-TOF): *m/z* 735 [M⁺], 708 [M⁺-C₂H₄], 679 [M⁺-C₂H₄]; Anal. calcd for C₅₂H₅₄N₄+H₂O: C, 82.94; H, 7.50; N, 7.44%. Found: C, 83.14; H, 7.60; N, 7.44.

Porphycene 8-H₂

Porphycene **7-H₂** was heated to 290 °C in the solid phase under vacuum for 30 min. After cooling to rt, **8-H₂** was obtained quantitatively. mp > 300 °C; ¹H NMR (400 MHz; CDCl₃, Me₄Si) δ_H, ppm 10.20 (s, 2H), 9.44 (d, 2H, *J* = 11 Hz, *meso*), 9.32 (d, 2H, *J* = 11 Hz, *meso*), 9.30 (s, 2H), 8.94 (s, 2H), 8.34 (m, 4H), 7.73 (m, 4H), 3.87 (t, 4H, *J* = 8 Hz, -CH₂C₅H₁₁), 3.33 (brs, 2H, NH), 2.32 (m, 4H, -CH₂CH₂C₄H₉), 1.76 (m, 4H, -C₂H₄CH₂C₃H₇), 1.59-1.41 (m, 8H, -C₃H₆CH₂C₂H₆ + -C₄H₈CH₂CH₃), 0.99 (t, 6H, *J* = 7 Hz, -C₃H₁₀CH₃); UV-vis (CH₂Cl₂): λ_{max}, nm (logε) 435 (4.88), 462 (5.15), 611 (4.37), 637 (4.68), 659 (5.00). HRMS (ESI): *m/z* 679.3802 (calcd. for C₄₈H₄₇N₄ [M+H]⁺ 679.3801).

Porphycene 1-Zn

A solution of **1-H₂** (30 mg, 0.048 mmol) and Zn(OAc)₂•2H₂O (300 mg, 1.4 mmol) in a mixture of CHCl₃ (20 ml), MeOH (15 ml) and TEA (1.0 ml) was heated at 50 °C for 15 h. The reaction mixture was washed with water and brine, dried over Na₂SO₄, and the solvent was concentrated under a reduced pressure. The crude product was purified by recrystallization from CHCl₃/MeOH to give **1-Zn** as a purple crystal. Yield 79% (26 mg, 0.038 mmol). Mp 162 °C (decomposed). ¹H NMR (400 MHz; CDCl₃, Me₄Si): δ_H, ppm 9.97 (s, 4H, *meso*), 7.25-7.14 (m, 8H, olefin), 6.10 (m, 4H, bridge head), 5.68 (m, 4H, bridgehead), 2.23-1.92 (m, 16H, bridge). UV-vis (pyridine): λ_{max}, nm (logε) 391 (4.85), 595 (4.35), 638 (5.00). MS (MALDI-TOF) *m/z*: 684 [M⁺], 656 [M⁺-C₂H₄], 628 [M⁺-

2C₂H₄], 600 [M⁺-3C₂H₄], 573 [M⁺-4C₂H₄]. Anal. calcd for C₄₄H₃₆N₄Zn+1/4CHCl₃: C, 74.22; H, 5.10; N, 7.82%. Found: C, 74.18; H, 5.18; N, 7.85.

Porphycene 2-Zn

1-Zn was heated to 200 °C in the solid phase under vacuum for 30 min. After cooling to rt, **2-Zn** was obtained quantitatively as a green solid. mp > 300 °C; ¹H NMR (400 MHz; C₅D₅N) δ_H, ppm 10.59 (s, 4H, *meso*), 10.27 (m, 4H, benzo), 9.75 (m, 2H, benzo), 8.27 (m, 4H, benzo), 8.21 (m, 4H, benzo). UV (pyridine): λ_{max}, nm (logε) 445 (5.56), 449 (5.54), 603 (4.26), 652 (5.19); MS (MALDI-TOF): *m/z* 572 [M⁺]. Anal. calcd for C₃₆H₂₀N₄Zn: C, 75.33; H, 3.51; N, 9.76%. Found: C, 75.38; H, 3.76; N, 9.74.

Porphycene 4-Zn

A solution of **4-H₂** (16 mg, 28 μmol) and Zn(OAc)₂ (50 mg) in DMF (5 ml) was refluxed for 3 h. After cooling to rt, the reaction mixture was diluted with CH₂Cl₂, and washed with water and brine, dried over Na₂SO₄. After a removal of the solvent, crystallization from CH₂Cl₂/MeOH gave **4-Zn** as a green solid. Yield 83% (15 mg, 23 μmol). ¹H NMR (400 MHz; C₅D₅N) δ_H, ppm 10.44 (d, 2H, *J* = 12 Hz, *meso*), 10.21 (m, 2H, benzo), 10.20 (d, 2H, *J* = 12 Hz, *meso*), 9.72 (m, 2H, benzo), 9.46 (s, 2H, β-H), 8.26 (m, 2H, benzo), 8.18 (m, 2H, benzo), 4.20 (t, 4H, *J* = 7.6 Hz, -CH₂C₅H₁₁), 2.44 (m, 4H, -CH₂CH₂C₄H₉), 1.77 (m, 4H, -C₂H₄CH₂C₃H₇), 1.49 (m, 4H, -C₃H₆CH₂C₂H₅), 1.38 (m, 4H, -C₄H₈CH₂CH₃), 0.91 (t, 6H, *J* = 7.3 Hz, -C₅H₁₀CH₃). UV (pyridine): λ_{max}, nm (logε) 424 (5.31), 597 (4.32), 643 (5.11). HRMS (ESI): *m/z* 640.2544 (calcd. for C₄₀H₄₀N₄Zn [M]⁺ 640.2544).

Porphycene 5-Zn

A solution of **5-H₂** (14 mg, 1.7 μmol) and Zn(OAc)₂·2H₂O (337 mg, 2.1 mmol) in CHCl₃ (10 ml), MeOH (5 ml) and TEA (0.5 ml) was refluxed for 9 h. The solvent was concentrated under a reduced pressure. The crude product was purified by alumina column chromatography (CHCl₃) and crystallization from CHCl₃/MeOH to give **5-Zn** as a deep blue solid. Yield 86% (13 mg, 15 μmol). mp 240 °C. (400 MHz; CDCl₃) δ_H, ppm 10.05-9.93 (m, 4H, *meso*), 7.88-7.20 (m, 16H, aromatic), 6.61-6.43 (m, 4H, bridge head), 6.07-5.95 (m, 4H, bridge head), 2.58-2.17 (m, 16H, bridge). UV-vis (pyridine): λ_{max}, nm (logε) 392 (5.23), 598 (4.37), 642 (5.00). HRMS (ESI): *m/z* 885.2937 (calcd. for C₆₀H₄₅N₄Zn [M+H]⁺ 885.2936).

Porphycene 6-Zn

Porphycene **5-Zn** was heated to 300 °C in the solid phase under vacuum for 1 h. After cooling to rt, **6-Zn** was obtained quantitatively. mp > 300 °C; ¹H NMR and ¹³C NMR spectra were not recorded because of the poor solubility. UV-vis (pyridine): λ_{max}, nm (logε) 389 (4.39), 446 (4.54), 471 (4.84), 488 (4.77), 611 (4.11), 659 (4.79). HRMS (FAB): *m/z* 772.1603 (calcd. for C₅₂H₂₈N₄Zn [M]⁺ 772.1605).

Porphycene 8-Zn

A solution of **8-H₂** (11 mg, 16 μ mol) and Zn(OAc)₂ (50 mg) in DMF (10 ml) was refluxed for 7 h. After cooling to rt, the reaction mixture was diluted with CH₂Cl₂, and washed with water and brine, and dried over Na₂SO₄. After a removal of the solvent, crystallization from CH₂Cl₂/MeOH gave **4-Zn** as a dark green solid. Yield 81% (9 mg, 13 μ mol). ¹H NMR (400 MHz; C₅D₅N): δ_{H} , ppm 10.79 (s, 2H), 10.33 (d, 2H, J = 12.0 Hz, *meso*), 10.18 (s, 2H), 10.17 (d, 2H, J = 12.0 Hz, *meso*), 9.39 (s, 2H), 8.84 (m, 2H), 8.68 (m, 2H), 7.91-7.85 (m, 4H), 4.19 (t, 4H, J = 7.5 Hz, -CH₂C₅H₁₁), 2.45 (m, 4H, -CH₂CH₂C₄H₉), 1.77 (m, 4H, -C₂H₄CH₂C₃H₇), 1.49 (m, 4H, -C₃H₆CH₂C₂H₅), 1.37 (m, 4H, -C₄H₈CH₂CH₃), 0.91 (t, 6H, J = 7.3 Hz, -C₄H₈CH₂CH₃). UV-vis (pyridine): λ_{max} , nm (log ϵ) 389 (4.39), 446 (4.54), 471 (4.84), 488 (4.77), 611 (4.11), 659 (4.79). HRMS (FAB): m/z 740.2854 (calcd. for C₄₈H₄₄N₄Zn [M]⁺ 740.2857).

X-ray Analysis

The selected single crystal was mounted in a Lindemann glass capillary with a tiny amount of the mother liquor. Single crystal X-ray diffraction analysis was performed at room temperature on a Rigaku AFC7S with a Cu target. The diffraction data were processed with CrystalStructure, solved with SIR-97 [33] and refined with SHELX-97 [34]. In the event of the solvent molecules not being adequately modeled, the structure of core porphyrin molecules were refined without the solvent molecules by the combination of the SHELX-97 and PLATON SQUEEZE programs.

Crystal data for **2-H₂** (C₃₆H₂₂N₄): M_w = 510.60, triclinic $P\bar{1}$, a = 5.5360(2), b = 14.5019(6), c = 14.7539(6) Å, α = 98.633(3)°, β = 91.079(2)°, γ = 96.534(3)°, V = 1162.67(8) Å³, T = 100(2) K, Z = 2. 13165 reflections were measured, and R_{merge} = 0.0757, R_1 = 0.0668 (2812, $I > 2\sigma(I)$), $wR_2(\text{all})$ = 0.1924 (4179), GOF = 1.054.

Crystal data for **4-H₂** (C₄₀H₄₂N₄): M_w = 578.80, monoclinic $P2_1/n$, a = 4.8635(16), b = 17.439(6), c = 36.083(12) Å, β = 93.174(3)°, V = 3055.7(18) Å³, T = 100(2) K, Z = 4. 18542 reflections were measured, and R_{merge} = 0.0564, R_1 = 0.0786 (6162, $I > 2\sigma(I)$), $wR_2(\text{all})$ = 0.0786 (6981), GOF = 1.066.

Crystal data for **2-Zn** (C₄₁H₂₅N₅Zn): M_w = 653.06, trigonal $R\bar{3}$, a = 27.642(4), b = 27.642(4), c = 19.628(3) Å, γ = 120.00°, V = 12988(4) Å³, T = 100(2) K, Z = 18. 8945 reflections were measured, and R_{merge} = 0.0186, R_1 = 0.0420 (5431, $I > 2\sigma(I)$), $wR_2(\text{all})$ = 0.0915 (6503), GOF = 1.115.

CONCLUSION

A series of benzoporphycenes and naphthoporphycenes and their zinc complexes were prepared from bicyclo[2.2.2]octadiene-fused porphycenes by retro-Diels-Alder reaction. Free-base porphycene showed drastic change of the fluorescence emission by the retro Diels-Alder reaction of the precursor to π -expanded porphycenes. However, both of the zinc BCOD porphycenes and π -

expanded porphycenes showed moderate fluorescence emission. The X-ray crystal structure of free-base tetrabenzoporphycene and dibenzoporphycene showed herringbone structure, which is promising structure for organic semi-conducting devices. On the contrary the zinc tetrabenzoporphycene made a hexahedral box-structure with six coordinated pyridine molecules inside.

ACKNOWLEDGEMENTS.

Authors thank the Venture Business Laboratory of Ehime University, for its help on TOF-MS spectroscopy. The present study was partly supported by a Grant-in-Aid (No. 22350083 for H.Y.) and the Green Photonics Project in NAIST (for H.Y. and D.K.) sponsored by the Ministry of Education, Culture, Sports, Science and Technology, Japan, and JSPS for a Research Fellowship for Young Scientists (for D.K.). We appreciate the Nippon Synthetic Chem. Ind. (Osaka Japan) for a gift of ethyl isocyanoacetate, which was used in preparation of the starting pyrroles.

SUPPORTING INFORMATION.

Figures S1-S16 (17 pages) are shown in supplementary information. This material is available at <http://www.u-bourgogne.fr/jpp/>. CCDC-823540 (**4-H₂**), CCDC-823541 (**2-H₂**), and CCDC-823542 (**2-Zn**) contain the supplementary crystallographic data for this paper. These data can be obtained free of charge from The Cambridge Crystallographic Data Centre via www.ccdc.cam.ac.uk/data_request/cif.

REFERENCES

1. Vogel E, Köcher M, Schmickler H, Lex J, *Angew. Chem. Int. Ed. Engl.* 1986; **25**: 257–259.
2. Sessler JL, Brucker EA, Schäfer M, Lex J, Vogel E, *Angew. Chem. Int. Ed. Engl.* 1994; **33**: 2308-2312.
3. Vogel E, Bröring M, Weghorn SJ, Scholz P, Deponte R, Lex J, Schmichler H, Schaffner K, Braslavsky SE, Müller M, Pörting S, Fowler CJ, Sessler JL, *Angew. Chem. Int. Ed. Engl.* 1997, **36**, 1651-1654.
4. Vogel E, Bröring M, Erben C, Demuth R, Lex J, Nendel M, Houk KN, *Angew. Chem. Int. Ed. Engl.* 1997, **36**, 353-357.
5. a) Sessler JL, Weghorn SJ, *Expanded, Contracted & Isomeric Porphyrins*. Elsevier, Oxford, 1997; b) Sessler JL, Gebauer A, Vogel E, *The Porphyrin Handbook* ed. Kadish KM, Smith KM and Guillard R, Academic Press: New York, 2000; vol. 2, 3–32.
6. a) Vogel E, *Pure Appl. Chem.* 1996; **68**: 1355; b) Vogel E, *J. Heterocyclic Chem.* 1996; **33**: 1461.

7. Sánchez-García D, Sessler JL, *Chem. Soc. Rev.* 2008; **37**: 215-232;
8. Vogel E, Balci M, Pramod K, Koch P, Lex J, Ermer O, *Angew. Chem. Int. Ed. Engl.* 1987; **26**: 928-931.
9. Vogel E, Koch P, Hou X-L, Lex J, Lausmann M, Kisters DCM, Aukauloo MA, Richard P, Guillard R, *Angew. Chem. Int. Ed. Engl.* 1993; **32**: 1600-1604.
10. Vogel E, Köcher M, Lex J, Ermer O, *Isr. J. Chem.* 1989; **29**: 257-266.
11. Nonell S, Bou N, Borrell J, Teixidó J, Villanueva A, Juarranz A, Cañete M, *Tetrahedron Lett.* 1995; **36**: 3405-3408; b) Gavalda A., Borrell J, Teixido J, Nonell S, Arad O, Grau R, Cañete M, Juarranz A, Villanueva A, Stockert JC, *J. Porphyrins Phthalocyanines* 2001; **5**: 846-852.
12. Vogel E, *Pure Appl. Chem.* **1993**; **65**: 143-152.
13. a) Roznyatovskiy V, Lynch V, Sessler JL, *Org. Lett.* 2010; **12**: 4424-4427. b) Sarma T, Panda PK, Anusha PT, Rao SV. *Org. Lett.* 2011; **13**: 188-191.
14. Masuno M, Robinson B, Phadke A, *J. Porphyrins Phthalocyanines* 2001; **5**: 177-180.
15. Dietrich HJ, *PhD Thesis, University of Cologne*, 1994.
16. a) Richert C, Wessels JM, Müller M, Kisters M, Benninghaus T, Goetz AE, *J. Med. Chem.* 1994; **37**: 2797-2807; b) Braslavsky SE, Müller M, Mártire DO, Pörting S, Bertolotti SG, Chakravorti S, Koç-Weier G, Knipp B, Schaffner K, *J. Photochem. Photobio, B* 1997; **40**: 191-198.
17. Ito S, Murashima T, Ono N, Uno H, *Chem. Commun.* 1998; 1661-1662.
18. Ono N, Yamada H, Okujima T, *Handbook of Porphyrin Science*, ed. Kadish, Karl M, Kevin M. Smith, Roger Guillard, World Scientific Publication Co. Pte. Ltd: Singapore, 2010, Vol. 2 1-102
19. Ito S, Ochi N, Murashima T, Ono N, Uno H, *Chem. Commun.* 2000; 893-894
20. Yamada H, Kuzuhara D, Takahashi T, Shimizu Y, Uota K, Okujima T, Uno H, Ono N, *Org. Lett.* 2008; **10**: 2947-2950.
21. Nakamura J, Okujima T, Tomimori Y, Komobuchi N, Yamada H, Uno H, Ono N, *Heterocycles* 2010; **80**: 1165-1175.
22. a) Shimizu Y, Shen Z, Okujima T, Uno H, Ono N, *Chem. Commun.* 2004; 374-375; b) Okujima T, Komobuchi N, Shimizu Y, Uno H, Ono N, *Tetrahedron Lett.* 2004; **45**: 5461-5464; c) Mack J, Bunya M, Shimizu Y, Uoyama H, Komobuchi N, Okujima T, Uno H, Ito S, Stillman MJ, Ono N, Kobayashi N, *Chem. Eur. J.* 2008; **14**: 5001-5020.
23. a) Ono N, Kuroki K, Watanabe E, Ochi N, Uno H, *Heterocycles* 2004; **62**: 365-373; b) Okujima T, Kikkawa T, Kawakami S, Shimizu Y, Yamada H, Ono N, Uno H, *Tetrahedron* 2010; **66**: 7212-7218.
24. Yamada H, Okujima T, Ono N, *Chem. Commun.* 2008; 2957-2974.

25. Shea PB, Kanicki J, Pattison LR, Petroff P, Kawano M, Yamada H, Ono N, *J. Appl. Phys.* 2006; **100**: 034502.
26. Matsuo Y, Sato Y, Niinomi T, Soga I, Tanaka H, Nakamura E, *J. Am. Chem. Soc.* 2009; **131**: 16048-16050.
27. Kuzuhara D, Mack J, Yamada H, Okujima T, Ono N, Kobayashi N, *Chem. Eur. J.* 2009; **15**: 10060-10069
28. Kuzuhara D, Yamada H, Yano K, Okujima T, Mori S, Uno H. *Chem. Eur. J.* 2011; **17**: 3376-3383.
29. Frisch MJ, Trucks GW, Schlegel HB, Scuseria GE, Robb MA, Cheeseman JR, Montgomery JA, Vreven JT, Kudin KN, Burant JC, Millam JM, Iyengar SS, Tomasi J, Barone V, MennucciB, Cossi M, Scalmani G, N. Rega N, Petersson GA, Nakatsuji H, Hada M, Ehara M, Toyota K, Fukuda R, Hasegawa J, Ishida M, Nakajima T, Honda Y, Kitao O, Nakai H, Klene M, Li X, Knox JE, Hratchian HP, Cross JB, Adamo C, Jaramillo J, Gomperts R, Stratmann RE, Yazyev O, Austin AJ, Cammi R, Pomelli C, Ochterski JW, Ayala PY, Morokuma K, Voth GA, Salvador P, Dannenberg JJ, Zakrzewski VG, Dapprich S, Daniels AD, Strain MC, Farkas O, Malick DK, Rabuck AD, Raghavachari K, Foresman JB, Ortiz JV, Cui Q, Baboul AG, Clifford S, Cioslowski J, Stefanov BB, Liu G, Liashenko A, Piskorz P, Komaromi I, Martin RL, Fox DJ, T. Keith T, M. A. Al-Laham MA, C. Y. Peng CY, A. Nanayakkara A, M. Challacombe M, Gill PMW, Johnson B, Chen W, Wong MW, Gonzalez C, Pople JA, Gaussian 03 RC, Gaussian, Inc., Wallingford CT, **2004**.
30. a) Berman A, Michaeli A, Feitelson J, Bowman MK, Norris JR, Levanon H, Vogel E, Koch P. *J. Phys. Chem.* 1992 ; **96** : 3041-3047; b) Sobolewski AL, Gil M, Dobkowski J, Waluk J. *J. Phys. Chem. C* 2009 ; **113**: 7714-7716.
31. Vogel E, Koch P, Hou XL, Lex J, Lausmann M, Kisters M, Aukauloo MA, Richard P, R. Guillard R, *Angew. Chem.* 1993 ; **105**, 1670-1673; *Angew. Chem. Int. Ed. Engl.* 1993 ; **32** :1600-1603.
32. Uoyama H, Takiue T, Tominaga K, Ono N, Uno H, *J. Porphyrins Phthalocyanines* 2009; **13**: 122–135.
33. Altomare A, Burla MC, Camalli M, Cascarano G, Giacovazzo C, Guagliardi A, Moliterni AGG, Polidori G, Spagna R, *J. Appl. Crystallogr.* 1999; **32**: 115-118.
34. Sheldrick GM, *Acta Cryst.* 2008; **A64**: 112-122.

Figure and Tables Captions

Table 1. Absorption and fluorescence peaks and fluorescence quantum yields.

Scheme 1. *Reagents and conditions:* i) BTMA•ICl₂, CaCO₃, CH₂Cl₂, MeOH, reflux; ii) (Boc)₂O, DMAP, CH₂Cl₂, rt; iii) Cu powder, DMF, 110 °C; iv) conc. HCl, EtOAc, rt; v) NaOH, ethylene glycol, 170 °C; vi) DMF, POCl₃, CH₂Cl₂, reflux, then, NaOAc.

Scheme 2. *Reagents and conditions:* i) Zn, TiCl₄, CuCl, THF, reflux; ii) 290 °C.

Scheme 3. *Reagents and conditions:* i) Zn(OAc)₂•2H₂O, CHCl₃, MeOH, 50 °C; ii) 200 °C for **1-Zn**, 290 °C for **4-Zn**; iii) Zn(OAc)₂•2H₂O, DMF, reflux.

Figure 1. BCOD-fused porphycene, benzoporphycene and naphthoporphycene.

Figure 2. Thermogravimetric analysis of **5-H₂**.

Figure 3. Absorption spectra of **4-H₂** (dashed line), **7-H₂** (solid line), **8-H₂** (bold solid line) and **17** (dotted line) in CH₂Cl₂.

Figure 4. Fluorescence spectra of **4-H₂** (dashed line), **8-H₂** (solid line) and **17** (dotted line) in CH₂Cl₂, excited at B peaks.

Figure 5. Absorption spectra of **1-Zn** (solid line), **2-Zn** (dashed line), **5-Zn** (dotted broken line) and **6-Zn** (bold solid line) in pyridine.

Figure 6. Absorption spectra of **1-Zn** (dotted line), **4-Zn** (dashed line) and **8-Zn** (solid line) in pyridine.

Figure 7. Fluorescence spectra of (a) **1-Zn** (dotted line), **4-Zn** (dashed line), **5-Zn** (solid line) and **8-Zn** (bold solid line) and (b) **1-Zn** (dotted line), **4-Zn** (dashed line), **5-Zn** (solid line) and **8-Zn** (bold line), excited at B peaks in pyridine.

Figure 8. A single crystal structure of **2-H₂**. (a) Structure of molecule 1; (b) packing structure.

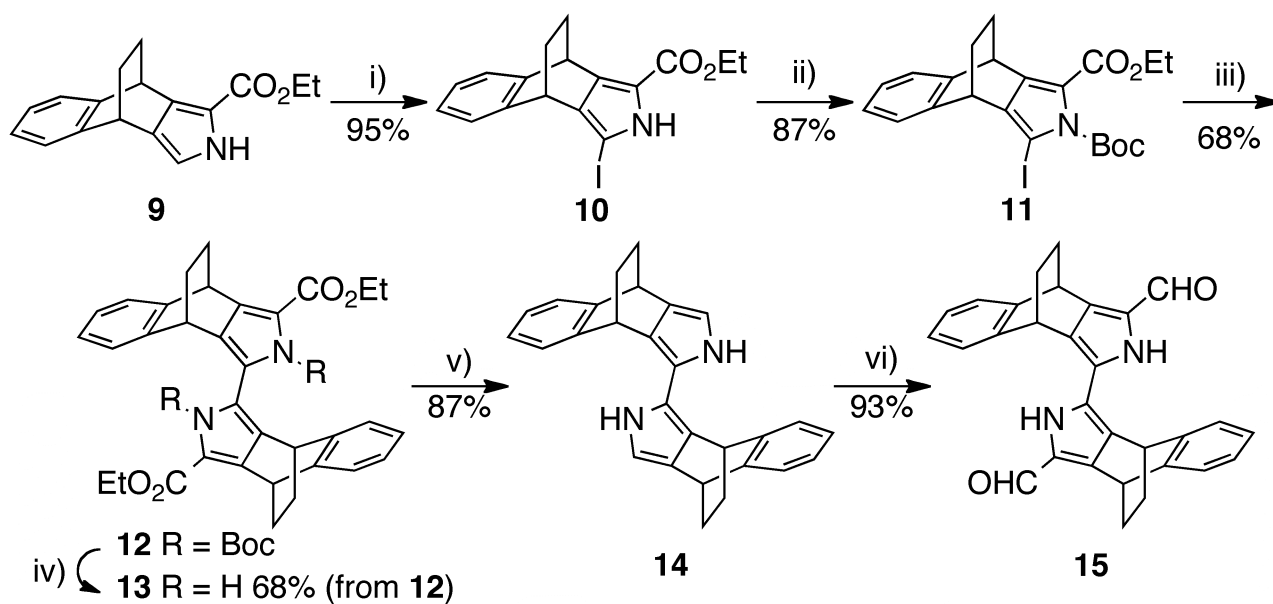
Figure 9. (a) A top view (The hexyl chain and hydrogen atoms expected for inner NH were omitted for clarity), (b) a side view, and (c) a packing structure of **4-H₂**.

Figure 10. (a) A top view, (b) a side view, and (c) a packing structure of **2-Zn**. Open arrow in (b) shows the direction to see top view.

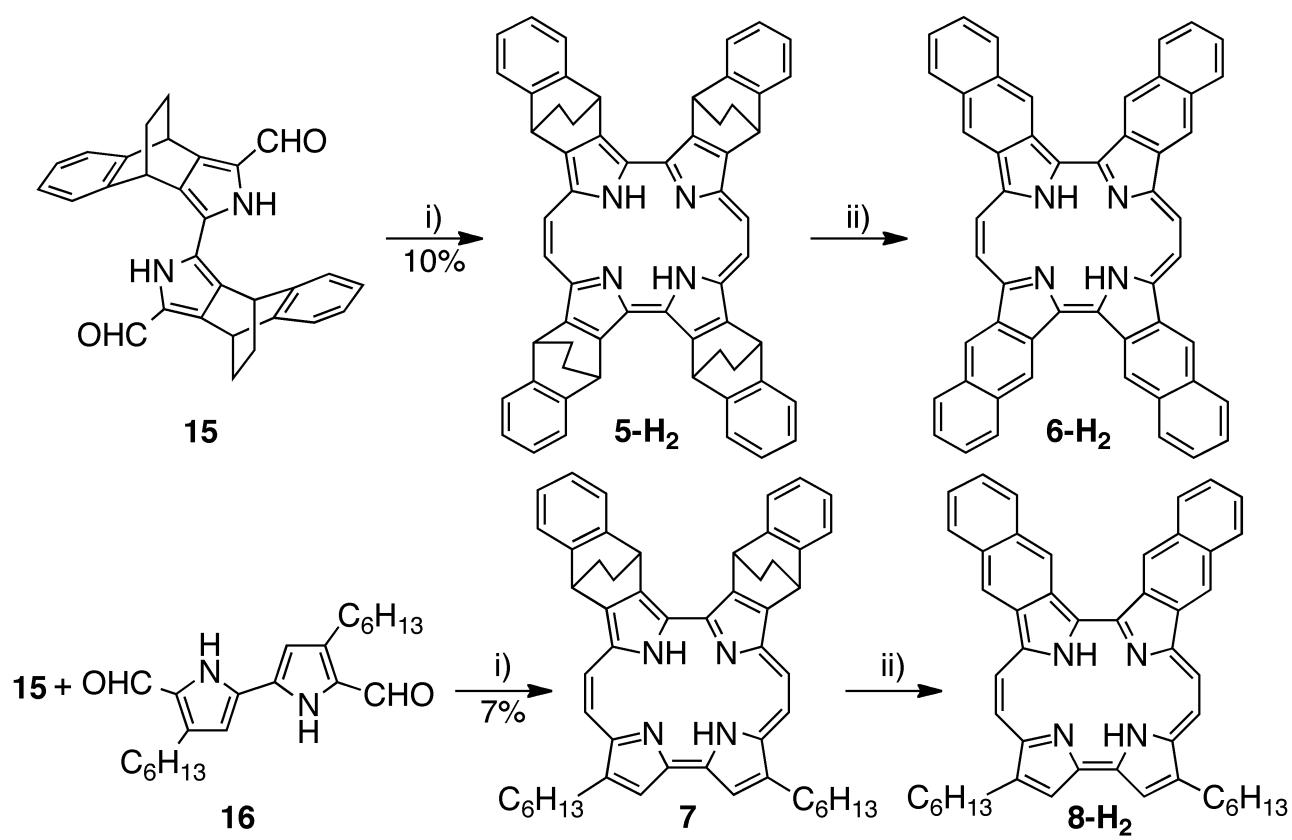
Table 1. Absorption and fluorescence peaks and fluorescence quantum yields.

	$\lambda_{\text{abs}} / \text{nm}^{\text{c)}$	$\lambda_{\text{em}} / \text{nm}^{\text{c)}$	$\Phi^{\text{c)}$		$\lambda_{\text{abs}} / \text{nm}^{\text{d)}$	$\lambda_{\text{em}} / \text{nm}^{\text{d)}$	$\Phi^{\text{d)}$
1-H₂^{a)}	374, 383 (sh), 568, 612, 646	n.d.	-	1-Zn	391, 595, 638	648, 701	0.26
2-H₂^{a)}	413, 434, 591, 627, 670	673, 752	0.32	2-Zn	445, 449 (sh), 603, 652	659, 724	0.37
3-H₂^{a)}	372, 382 (sh), 565, 606, 639	n.d.	-	3-Zn	-	-	-
4-H₂^{a)}	410, 573, 616, 647	654, 726	0.42	4-Zn	424, 597, 643	654, 709	0.31
5-H₂	373, 386, 573, 618, 652	661	0.002	5-Zn	392, 598, 642	656, 709	0.28
6-H₂^{b)}	-	-	-	6-Zn	476, 507, 586, 648, 685	696, 764	0.17
7-H₂	373, 384, 567, 609, 642	650	0.006	7-Zn	-	-	-
8-H₂	435, 462, 611, 637, 659	665, 733	0.31	8-Zn	388, 446, 471, 488, 611, 659	671, 735	0.15
17	371, 382, 563, 601, 633	639, 699	0.43	-	-	-	-

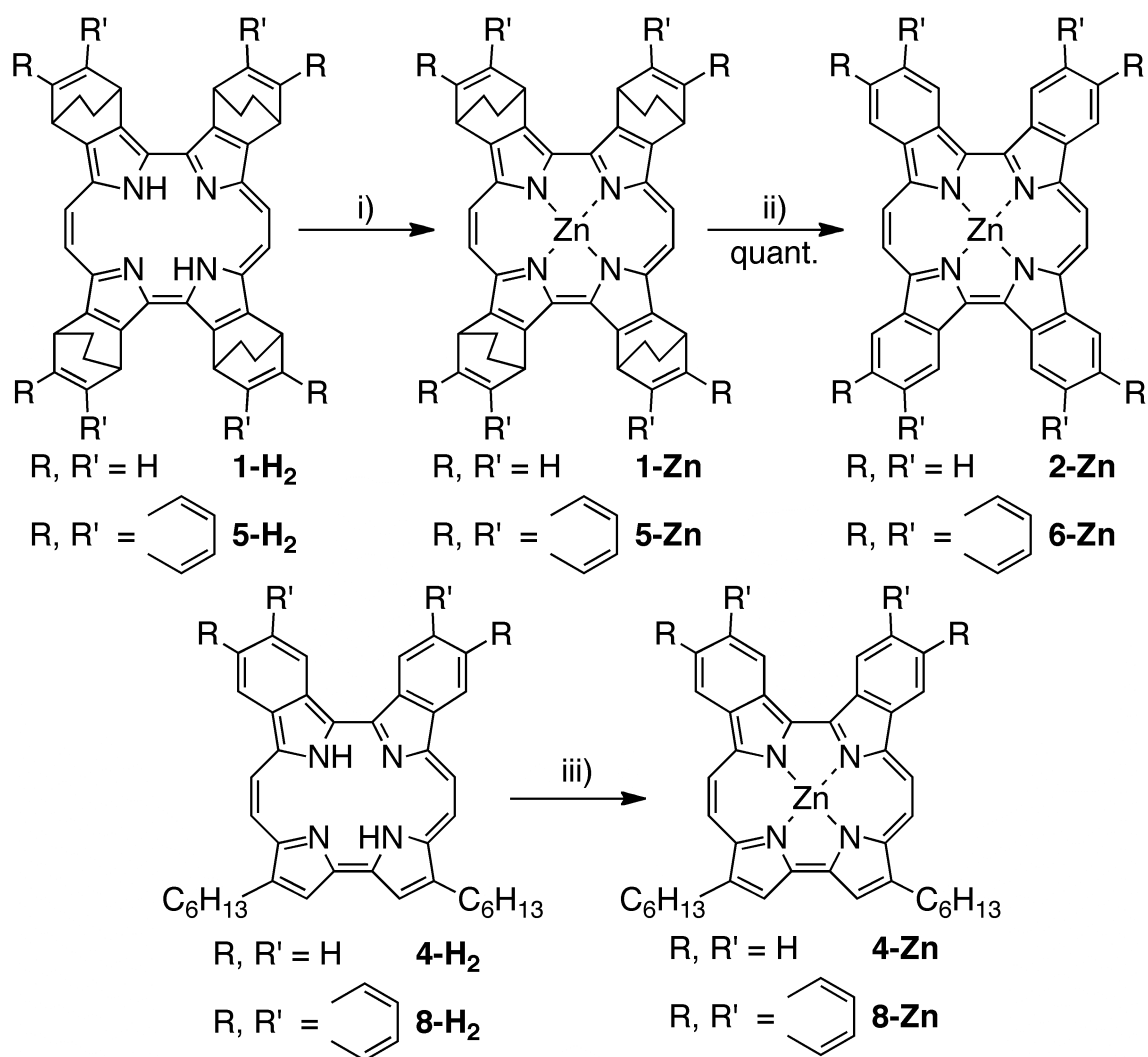
a): See in the literature 27; b): Data was not not collected due to very low-solubility of **6-H₂** in common organic solvent ; c) in CH₂Cl₂ ; d) in pyridine.



Scheme 1. Reagents and conditions: i) BTMA•ICl₂, CaCO₃, CH₂Cl₂, MeOH, reflux; ii) (Boc)₂O, DMAP, CH₂Cl₂, rt; iii) Cu powder, DMF, 110 °C; iv) conc. HCl, EtOAc, rt; v) NaOH, ethylene glycol, 170 °C; vi) DMF, POCl₃, CH₂Cl₂, reflux, then, NaOAc.



Scheme 2. Reagents and conditions: i) Zn, TiCl₄, CuCl, THF, reflux; ii) 290 °C.



Scheme 3. Reagents and conditions: i) $\text{Zn}(\text{OAc})_2$, $\bullet 2\text{H}_2\text{O}$ CHCl_3 , MeOH , $50\text{ }^\circ\text{C}$; ii) $200\text{ }^\circ\text{C}$ for **1-Zn**, $290\text{ }^\circ\text{C}$ for **4-Zn**; iii) $\text{Zn}(\text{OAc})_2$, $\bullet 2\text{H}_2\text{O}$, DMF , reflux.

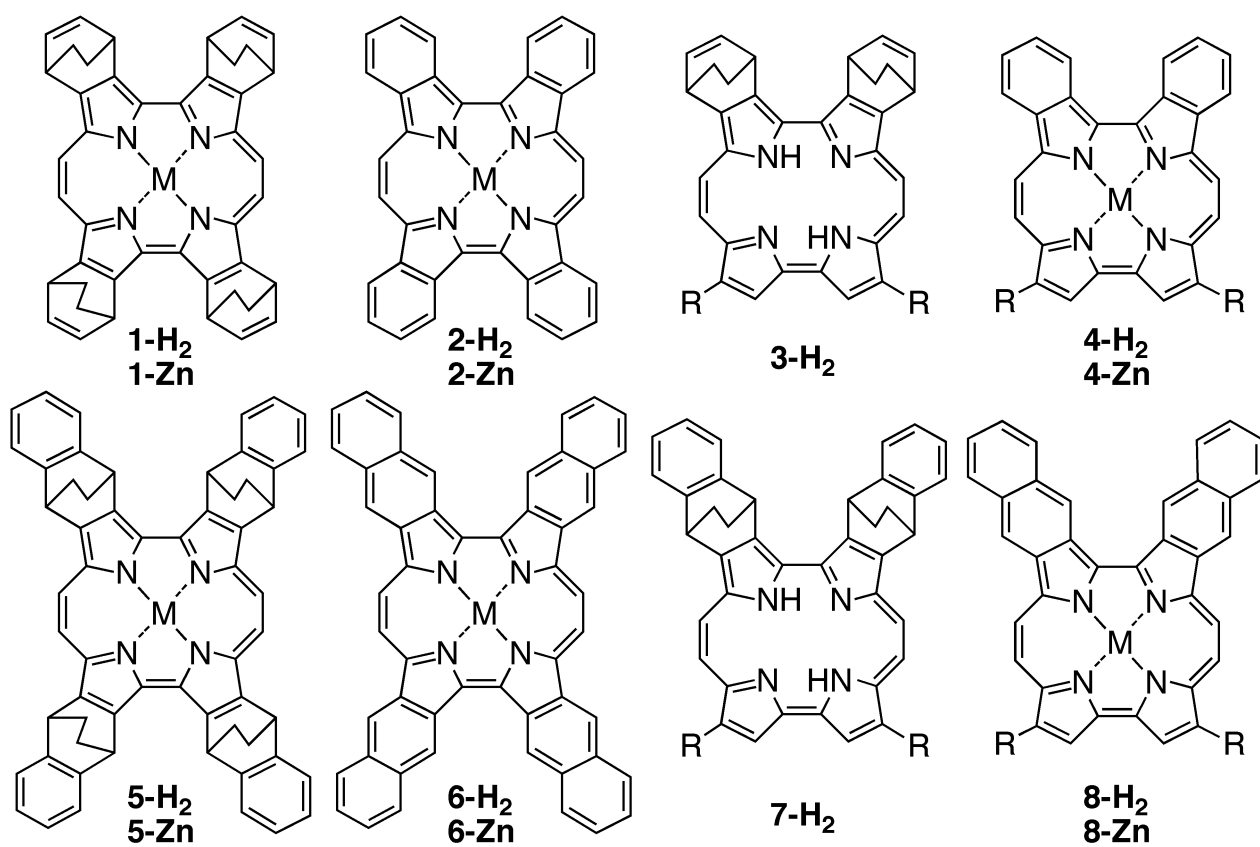


Figure 1 BCOD-fused porphycene, benzoporphycene and naphthoporphycene. ($R = C_6H_{13}$)

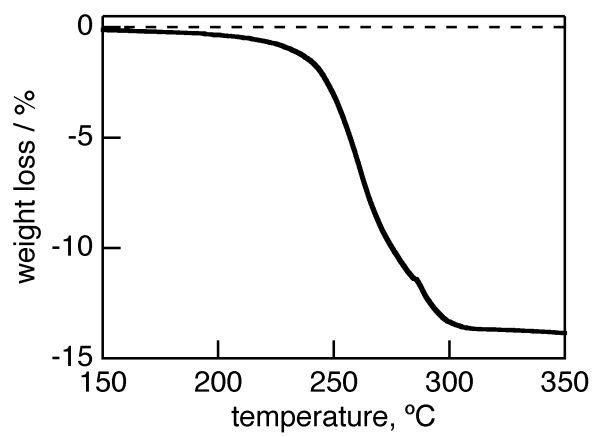


Figure 2. Thermogravimetric analysis of **5-H₂**.

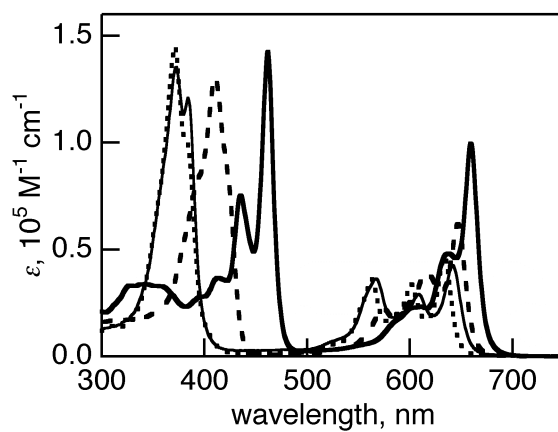


Figure 3. Absorption spectra of **4-H₂** (dashed line), **7-H₂** (solid line), **8-H₂** (bold solid line) and **17** (dotted line) in CH₂Cl₂.

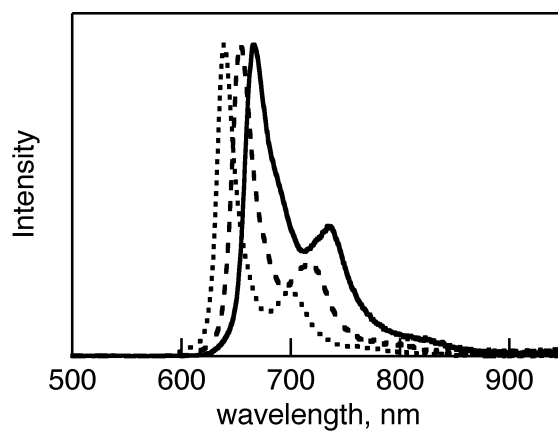


Figure 4. Fluorescence spectra of **4-H₂** (dashed line), **8-H₂** (solid line) and **17** (dotted line) in CH₂Cl₂, excited at B peaks.

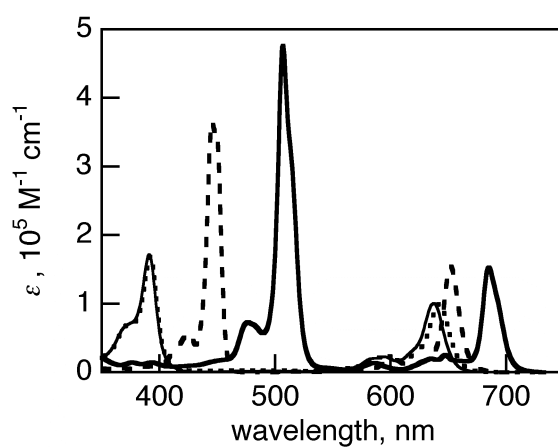


Figure 5. Absorption spectra of **1-Zn** (solid line), **2-Zn** (dashed line), **5-Zn** (dotted broken line) and **6-Zn** (bold solid line) in pyridine.

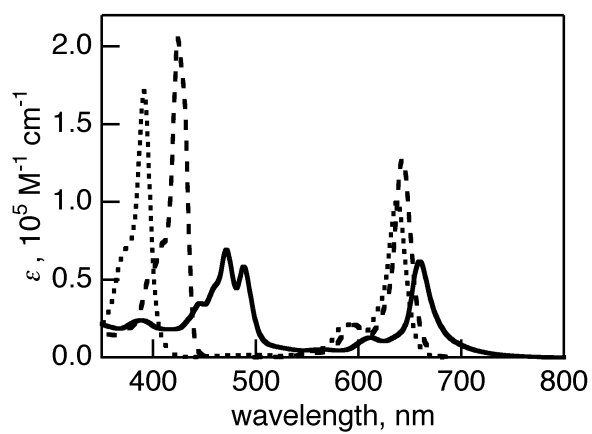


Figure 6. Absorption spectra of **1-Zn** (dotted line), **4-Zn** (dashed line) and **8-Zn** (solid line) in pyridine.

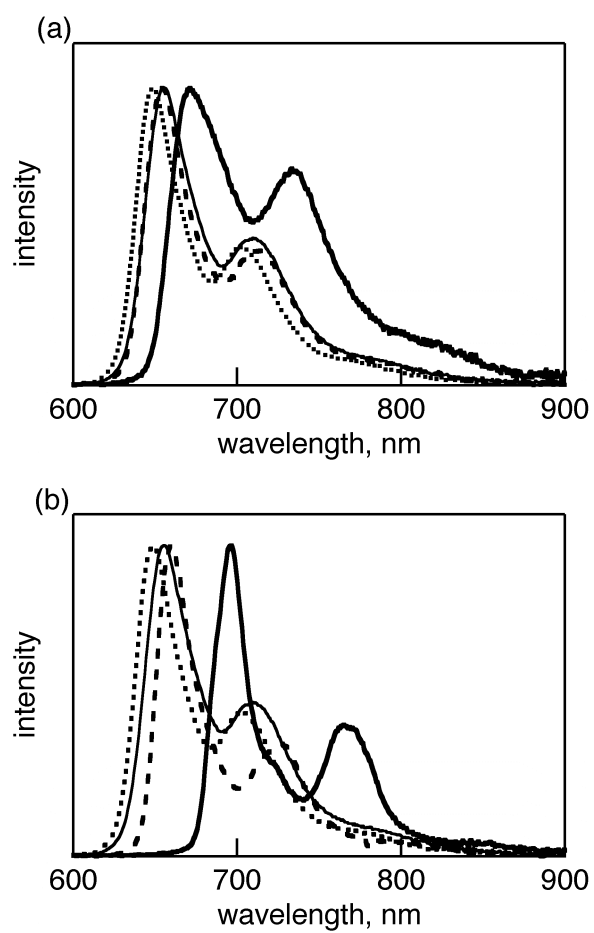


Figure 7. Fluorescence spectra of (a) **1-Zn** (dotted line), **4-Zn** (dashed line), **5-Zn** (solid line) and **8-Zn** (bold solid line) and (b) **1-Zn** (dotted line), **4-Zn** (dashed line), **5-Zn** (solid line) and **8-Zn** (bold line), excited at B peaks in pyridine.

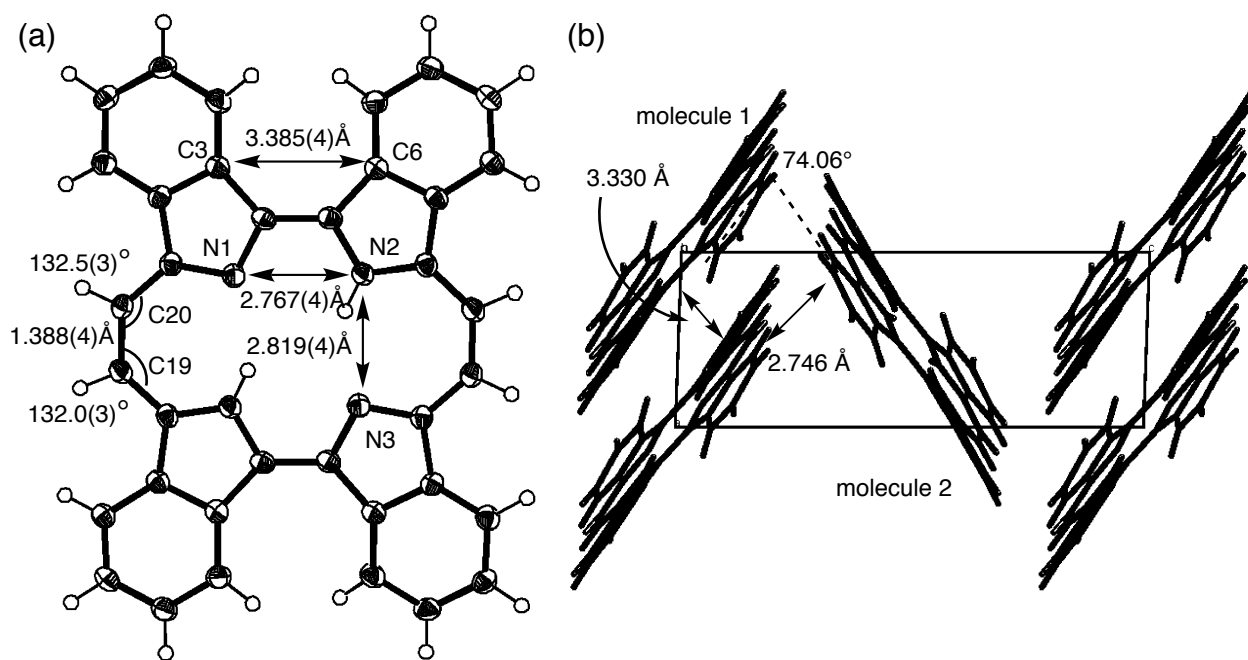


Figure 8. A single crystal structure of **2-H₂**. (a) Structure of molecule 1; (b) packing structure.

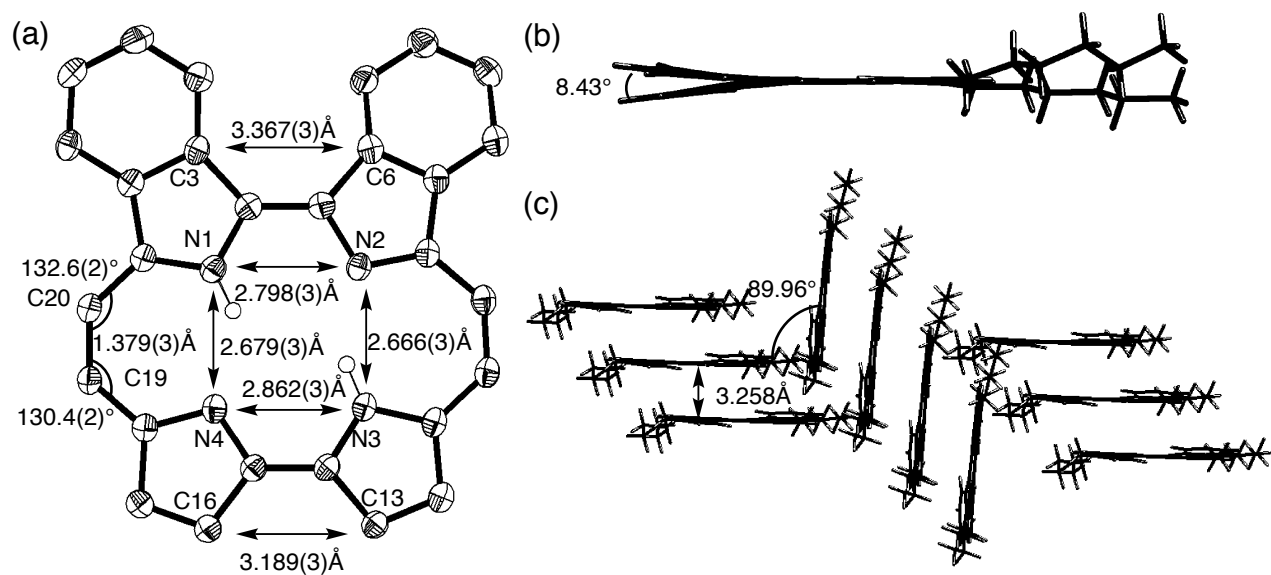


Figure 9. (a) A top view (The hexyl chain and hydrogen atoms expected for inner NH were omitted for clarity), (b) a side view, and (c) a packing structure of **4-H₂**.

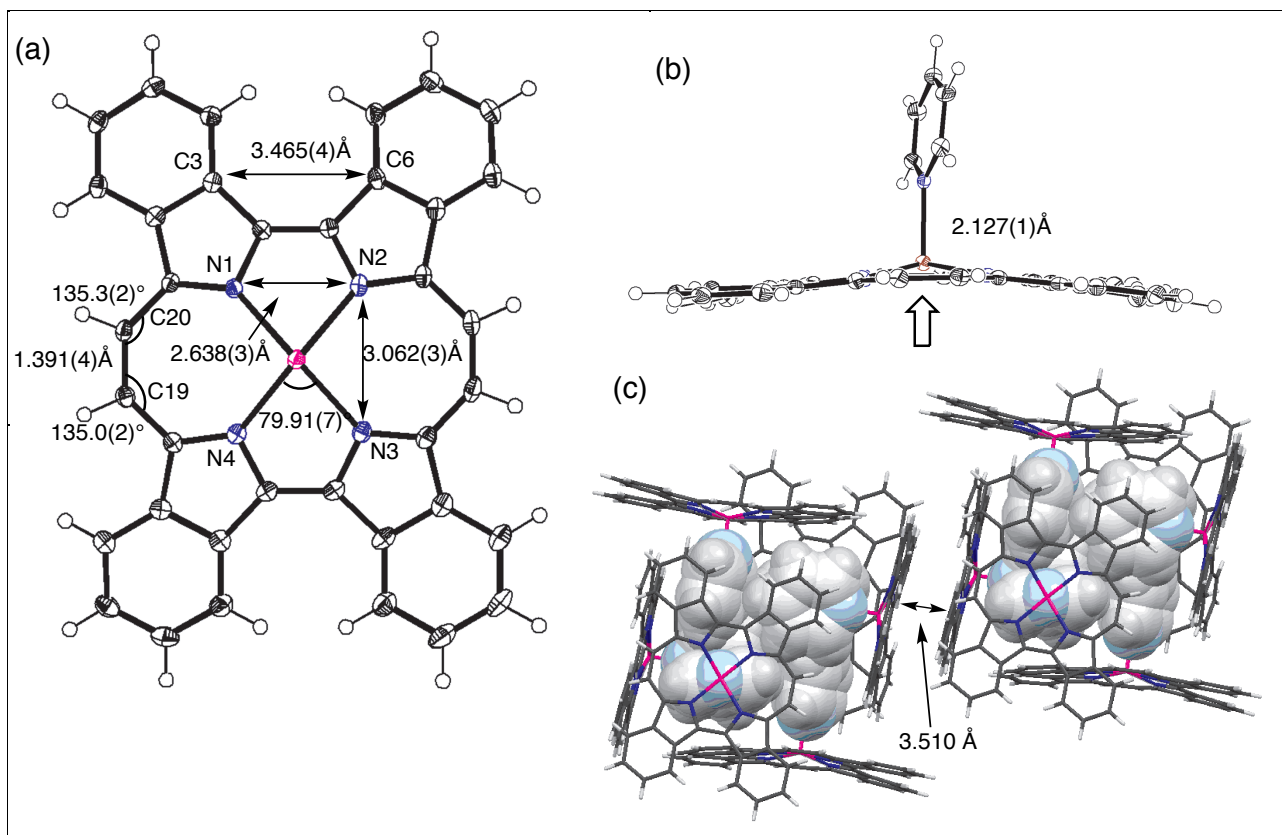


Figure 10. (a) A top view, (b) a side view, and (c) a packing structure of **2-Zn**. Open arrow in (b) shows the direction to see top view.

